Supporting Information

MOF-derived vertically stacked Mn_2O_3@C flakes for fiber-shaped zinc-ion batteries

Chenglong Liu[a,b], Qiulong Li[b,e], Hongzhao Sun[a,b], Zhen Wang[a,b], Wenbin Gong[b], Shan Cong[a,b,c,d], Yagang Yao[b,d,e], Zhigang Zhao[a,b,c,d]*

[a]School of Nano-Tech and Nano-Bionics, University of Science and Technology of China, Hefei 230026, China

[b]Key Lab of Nanodevices and Applications, Suzhou Institute of Nano-Tech and Nano-Bionics, Chinese Academy of Sciences, Suzhou 215123, China

[c]Key Laboratory of Multifunctional Nanomaterials and Smart Systems, Chinese Academy of Sciences, 215123 Suzhou, China

[d]Division of Nanomaterials, Suzhou Institute of Nano-Tech and Nano-Bionics, Chinese Academy of Sciences, 330200 Nanchang, China

[e]National Laboratory of Solid State Microstructures, College of Engineering and Applied Sciences, Jiangsu Key Laboratory of Artificial Functional Materials and Collaborative Innovation Center of Advanced Microstructures, Nanjing University, Nanjing 210093, China

Materials. Manganese(II) nitrate tetrahydrate ($Mn(NO_3)_2·4H_2O$, 98%), trimesic acid ($C_6H_3(COOH)_3$, 98%)，lauric acid ($C_{12}H_{24}O_2$, 98%), zinc sulfate heptahydrate ($ZnSO_4·7H_2O$, 99%), manganese sulfate monohydrate ($MnSO_4•H_2O$, 99%), PVA ($[CH_2CH\ (OH)]n$, n = 1799), methanol (CH_4O, 99.5%), ethanol (C_2H_6O, AR) were bought from Aladdin. Each of these chemicals was used directly without any further purification.

Synthesis of aligned CNT sheet. The aligned CNT array was prepared by chemical vapor deposition (CVD) in a tube furnace，and the catalyst was Fe/Al_2O_3 (1.5nm/ 5 nm) on a silicon substrate. The carbon source was Ethylene (90 sccm), and a mixture gas of Ar/H_2 (400 sccm/30 sccm) was used as the carrier gas. The growth time and temperature were 10 min and 740°C.

Materials characterization. The morphologies of the as-prepared samples were characterized by scanning electron microscopy (SEM; Hitachi S-4800, 5 kV). The microstructures of the samples were observed by transmission electron microscopy (TEM; FEI Tecnai G2 F20 S-Twin), and high-resolution TEM images were acquired on a FEI Tecnai G2 20 high-resolution transmission electron microscope operating at an acceleration potential of 200 kV. The chemical compositions of the samples were analyzed on an ESCALAB MKII X-ray photoelectron spectrometer (XPS) using non-monochromatized Mg Kα X-rays as the excitation source. X-ray diffraction (XRD) patterns were acquired on a Rigaku D/MAX2500 V system using Cu Kα radiation (λ= 1.5418 Å). The thermal decomposition behavior was studied by thermogravimetric analysis (TGA; Netzsch Instruments model 209 F1 Libra). The temperature was increased from 25 to 600℃ (the ramping rate was 10 °C/min) and the atmosphere is nitrogen . The Raman spectra are collected using an inVia Qontor confocal Raman spectrometer (Renishaw) with an excitation laser of 532.8 nm (0.02 mW). The laser spot is 1 mm in diameter.

Electrochemical Performance Measurements. The electrochemical performance of the as-fabricated samples was tested by galvanostatic charge-discharge, cyclic voltammetry and EIS measurements on an electrochemical workstation (CHI 760E,

Chenhua). The EIS measurements were carried out with the potential amplitude of 5 mV over the frequency range from 100 kHz to 0.01 Hz.

The volumetric capacity ($C_{V,cell}$, Ah cm^{-3}) is calculated by the following equations:

$$C_{V,cell} = \frac{I\Delta t}{V_{cell} \times 3600}$$

Where I, Δt, and V_{cell} are, respectively, the discharge current (A), the discharge time (s), and the volume of FESD device (cm^3).

The energy density (E_V, mW h cm^{-3}) is calculated by the following equation:

$$E_V = C_{V,cell} * V_P$$

The power density (P_V, mW cm^{-3}) is calculated by the following equation:

$$P_V = 3600\frac{E_V}{\Delta t}$$

Where V_p and Δt are, respectively, the voltage platform (V), the discharge time (s).

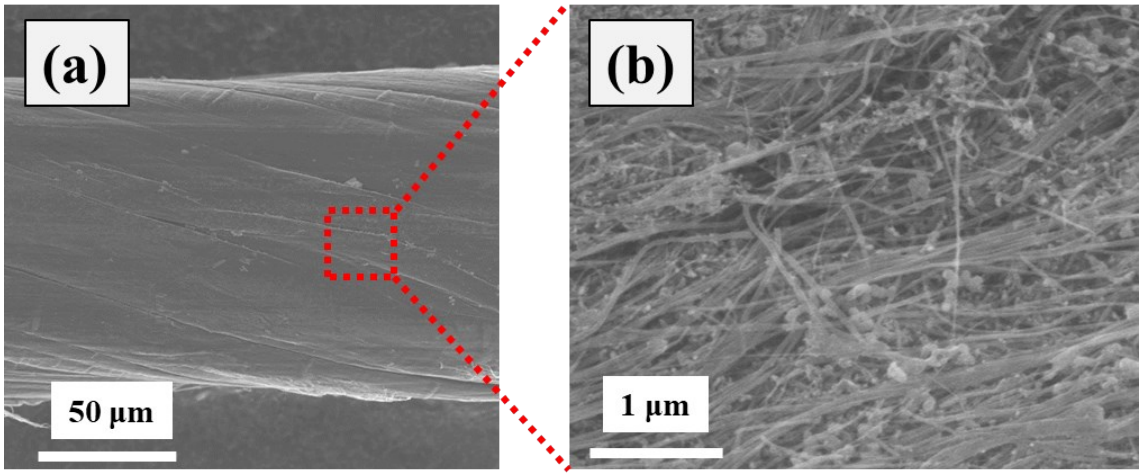

Figure S1. (a-b) SEM images of bare CNTF at different magnifications.

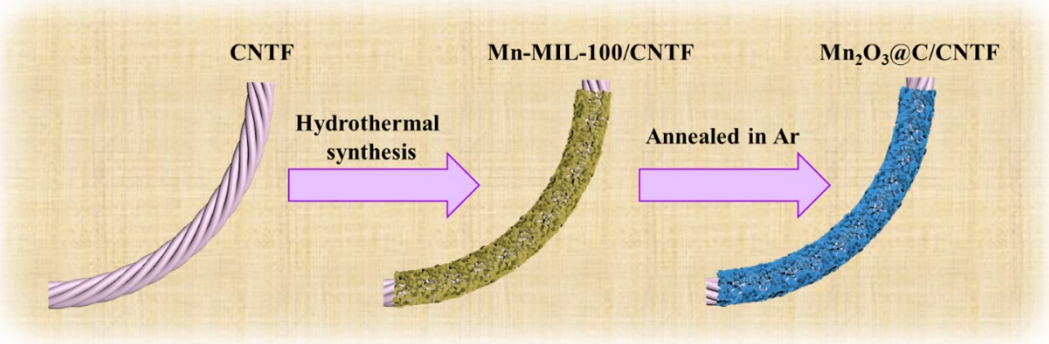

Figure S2. Schematic fabrication process of the Mn_2O_3@C/CNTF electrode.

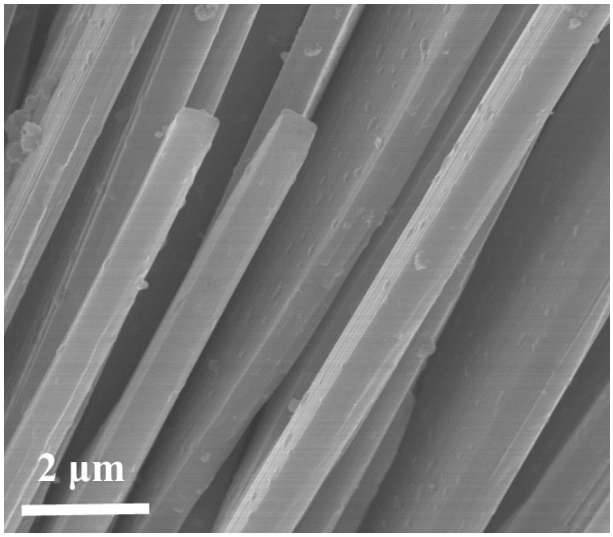

Figure S3. SEM image of Mn-MIL-100 /CNTF at high magnification.

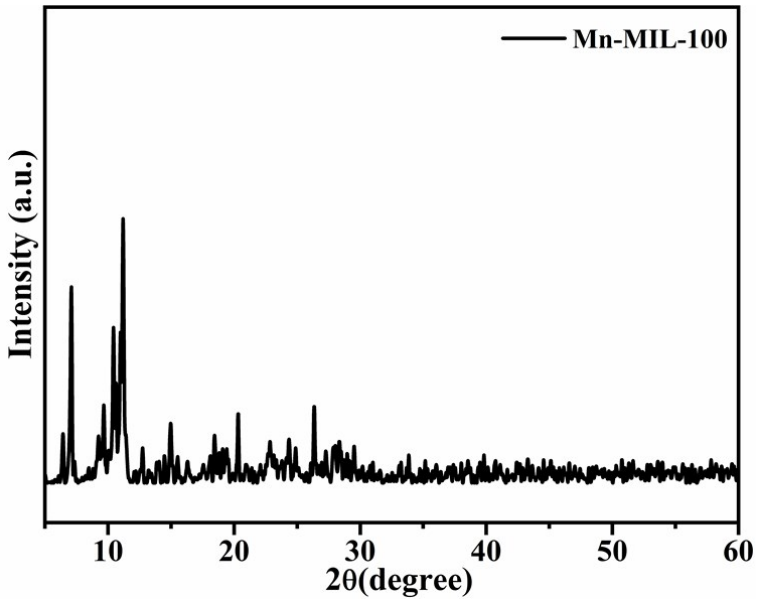

Figure S4. XRD patterns of Mn-MIL-100

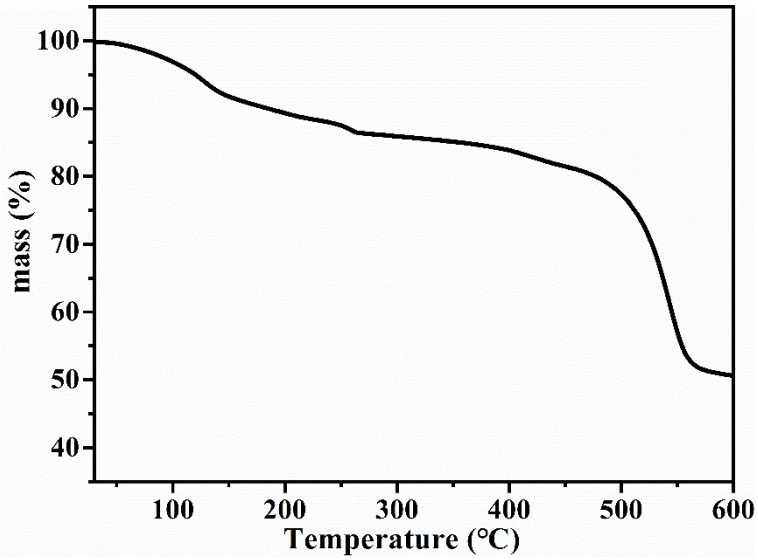

Figure S5. TGA curves of the Mn-MIL-100.

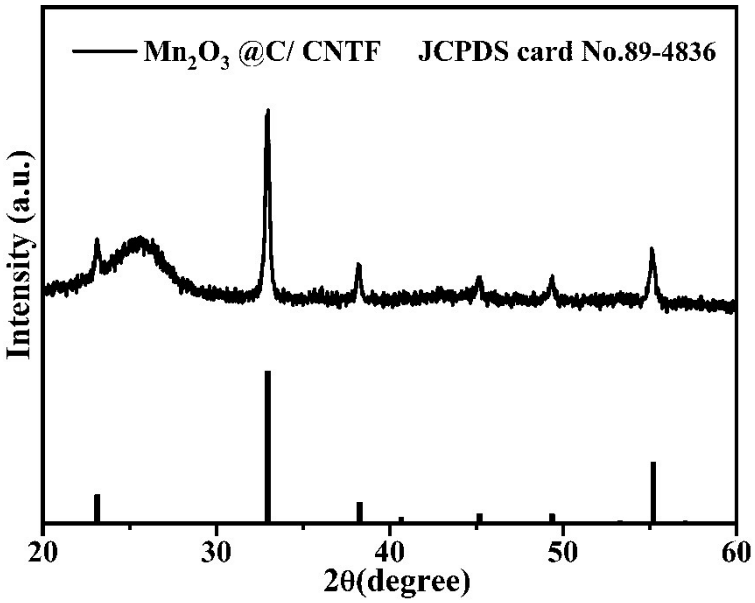

Figure S6. XRD patterns of the Mn_2O_3@C sample.

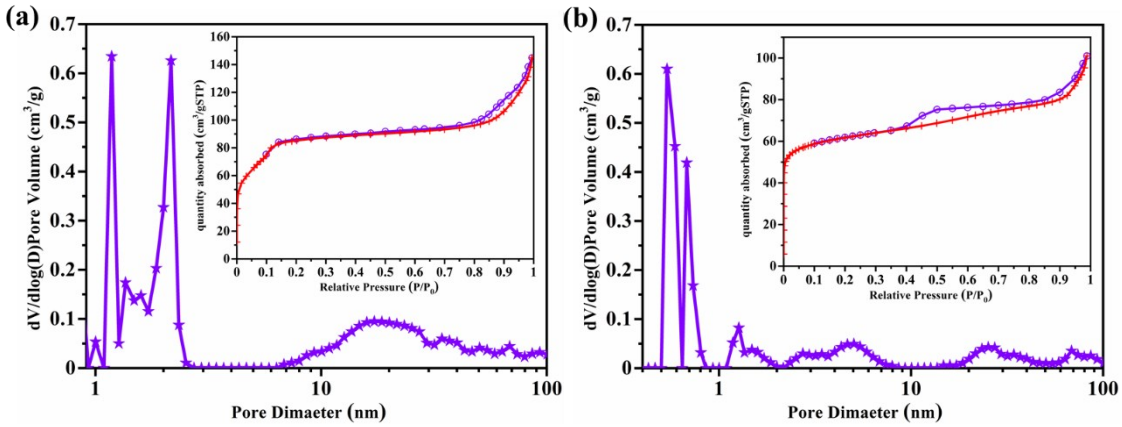

Figure S7. (a) BJH desorption pore distribution of Mn-MIL-100 materials. (Inset: N_2 absorption-desorption isotherm.) (b) BJH desorption pore distribution of Mn_2O_3@C electrode materials. (Inset: N_2 absorption-desorption isotherm.)

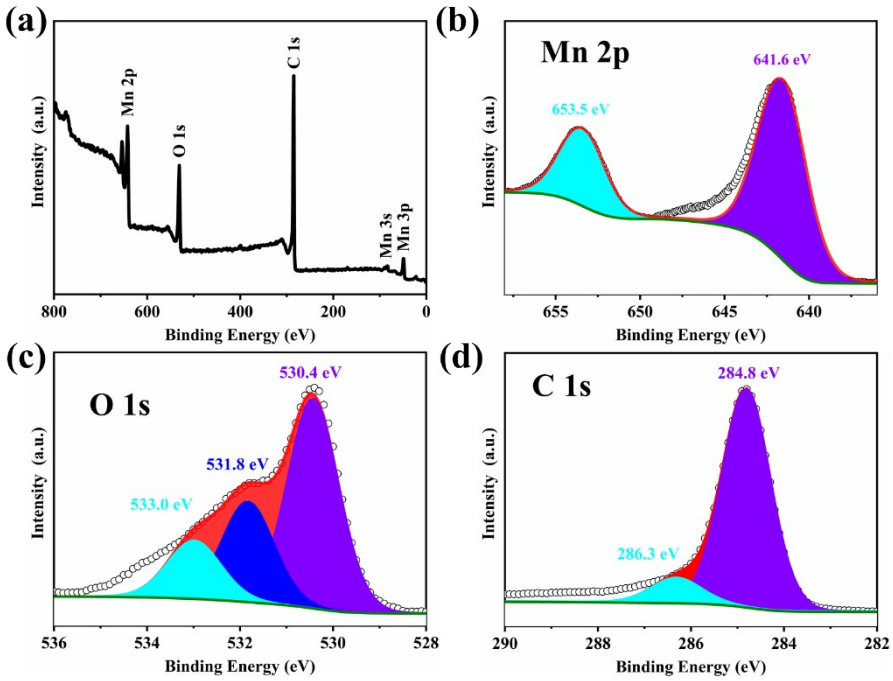

Figure S8. (a) XPS survey spectrum of the Mn_2O_3@C/ CNTF. (c) XPS survey spectrum of Mn 2p. (c) XPS survey spectrum of O 1s. (d) XPS survey spectra of the C 1s.

(a)

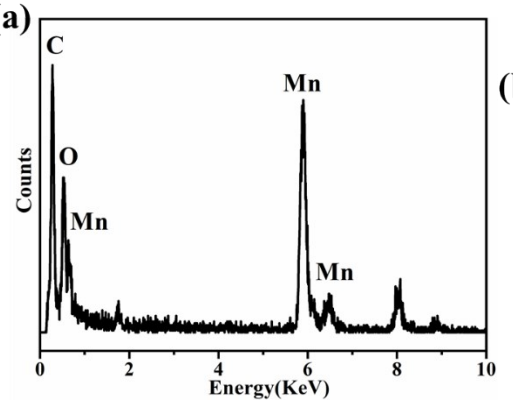

(b)

Element	C(K)	O(K)	Mn(K)
Weight %	55.69	13.54	30.76
Atomic %	76.72	14.00	9.26

Figure S9. EDS spectrum and element percentage of C, O and Mn of the Mn_2O_3@C/CNTF.

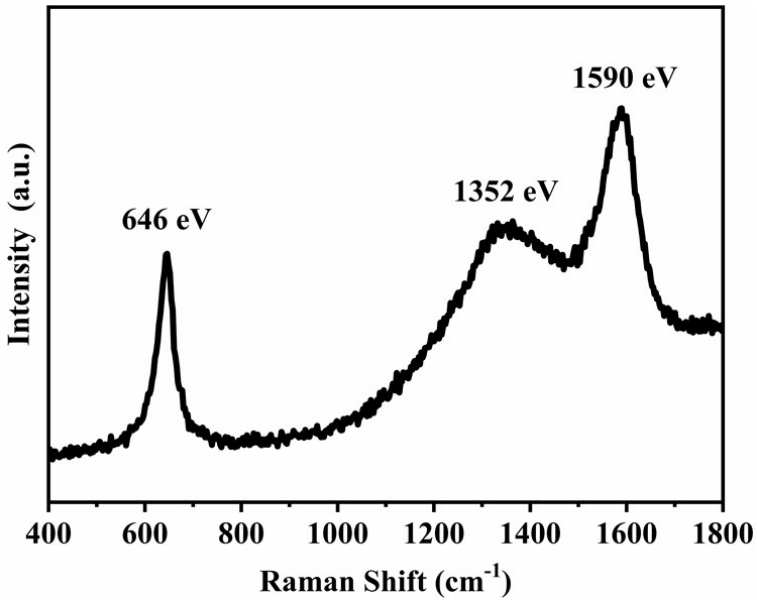

Figure S10. Raman spectrum of the Mn_2O_3@C/CNTF

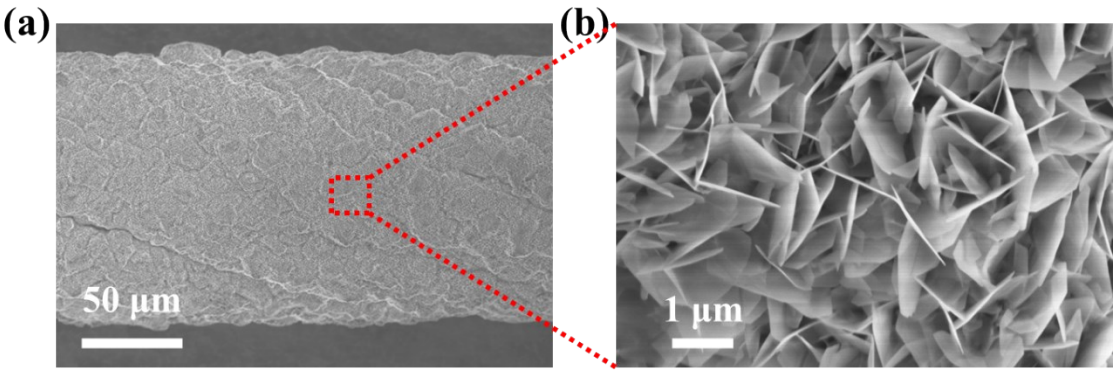

Figure S11. SEM images of Zn nanosheets on CNTF at different magnifications.

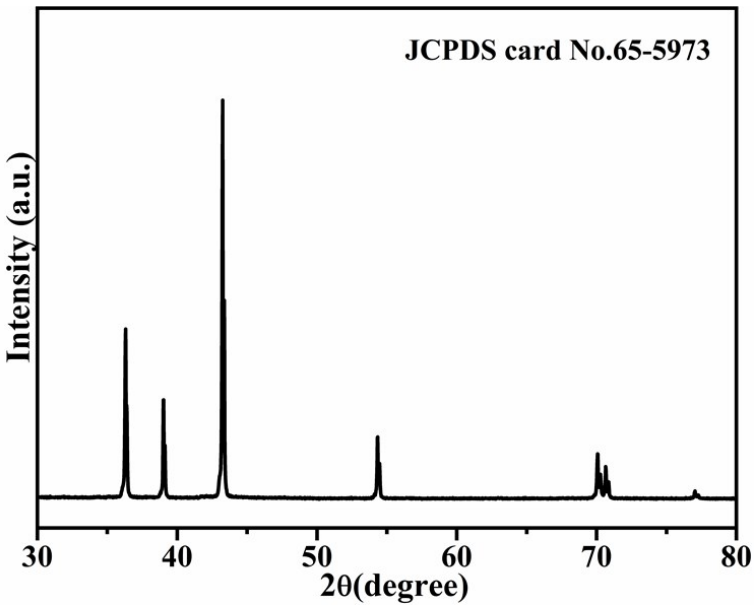

Figure S12. XRD patterns of Zn nanosheets

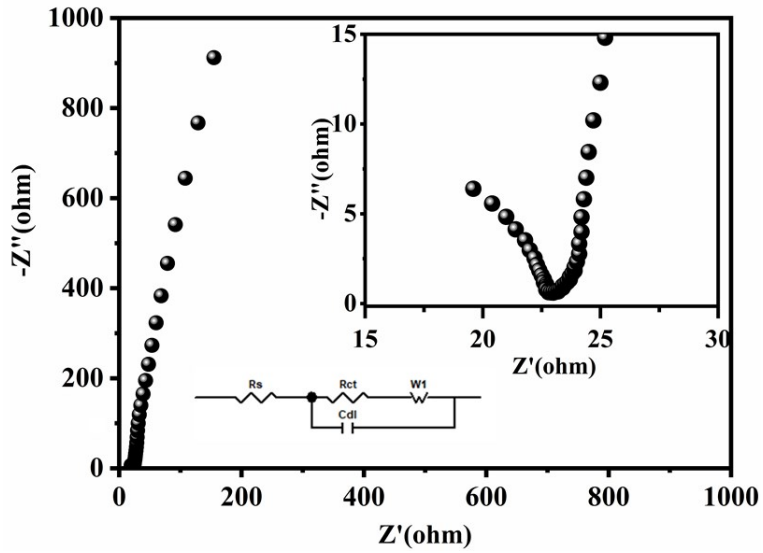

Figure S13. Nyquist plots of the single ZIBs device. The inset shows the high-frequency part of the Nyquist plots.

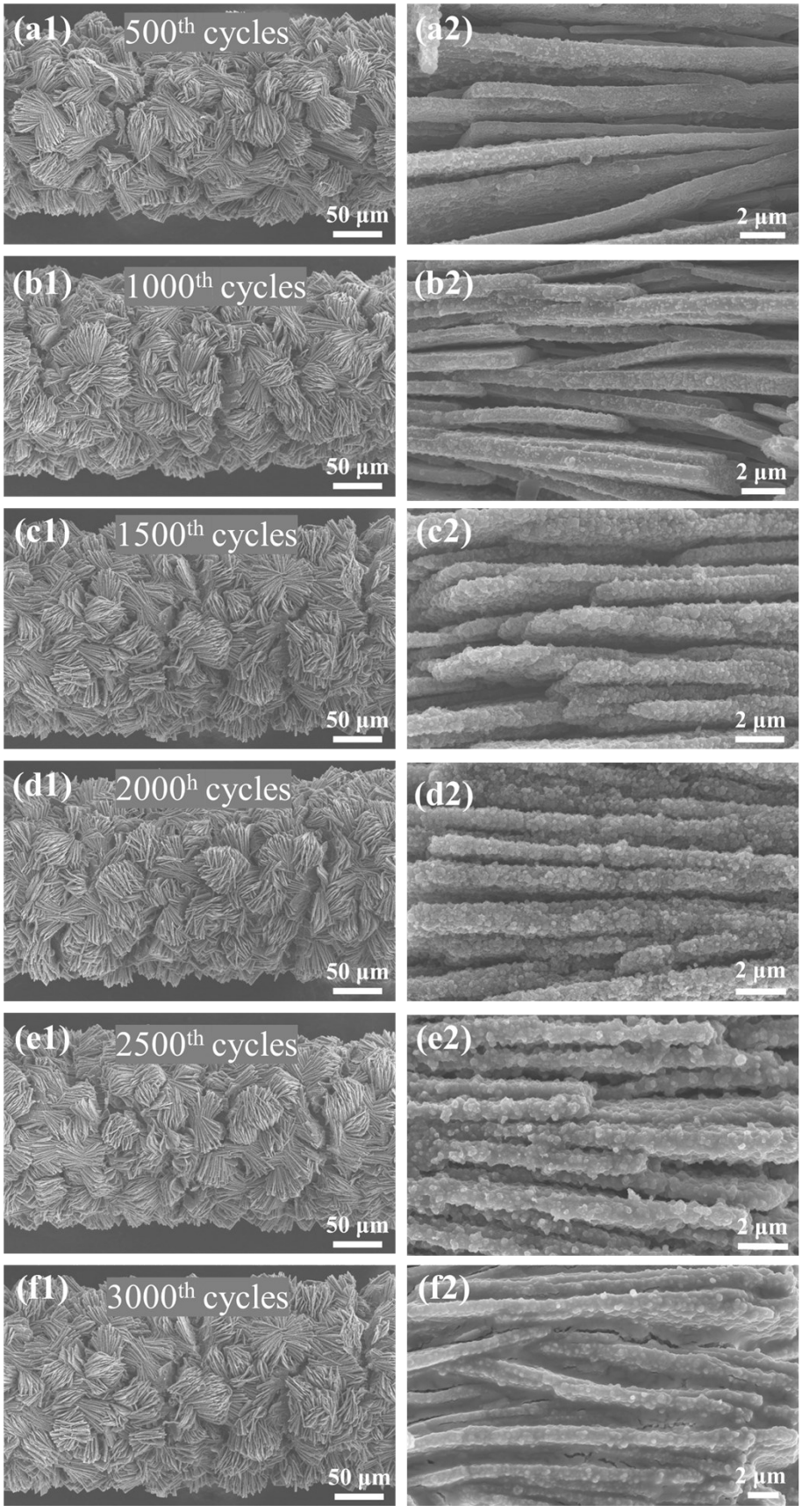

Figure S14. Low-magnification (a) and high-magnification (b) SEM images of the Mn_2O_3@C/CNTF at different cycles.

The free space between sheets could act as a buffer zone for volume change during the charge and discharge processes, which would effectively alleviate the structural damage to the electrode material caused by volume expansion. Another factor boosting the long-term cycling stability is that the porous structures provide not only free space for the accommodation of volume expansion but also channels for efficient Zn^{2+} diffusion. During the cycling process, the free space between sheets are gradually blocked along with the collapse of MOF-derived skeleton. The accumulations of electrode materials thus cause high internal resistance in cycling process, further hinder the reaction of internal electrode materials and reduce the capacity. Another reason may exist according to pervious report[1], that is the heterogeneous reaction in electrode materials with intermediate products gradually covering on the surface of the electrode materials, reducing the free space between sheets and blocking ion diffusion.

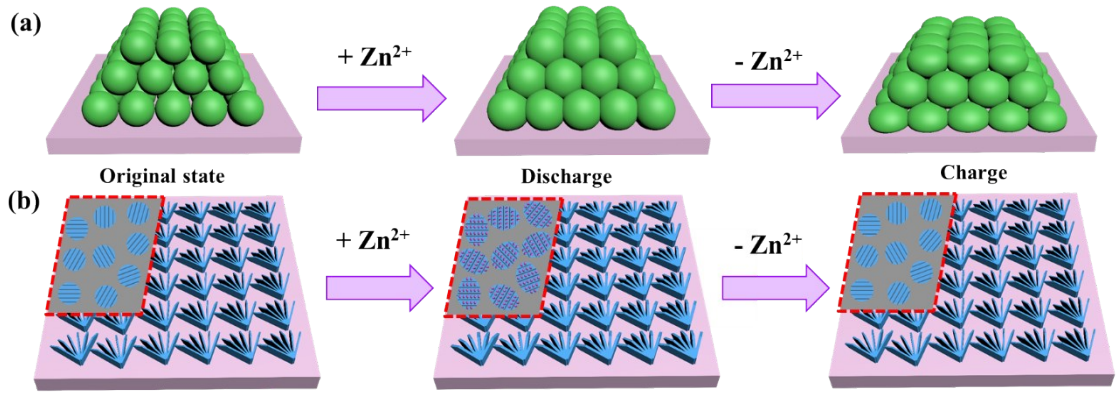

Figure S15. Schematic illustration of the superior cyclability of the 3D self-standing sheets array electrode compared to the traditional electrode materials. (a) Models of structure and effect of volume expansion for traditional graininess materials. (b) Models of structure and effect of volume expansion for 3D self-standing sheets array materials. (Inset: Models of the structure of Mn_2O_3 and C composite materials and the mechanisms of reducing the volume expansion for insertion of Zn ions.)

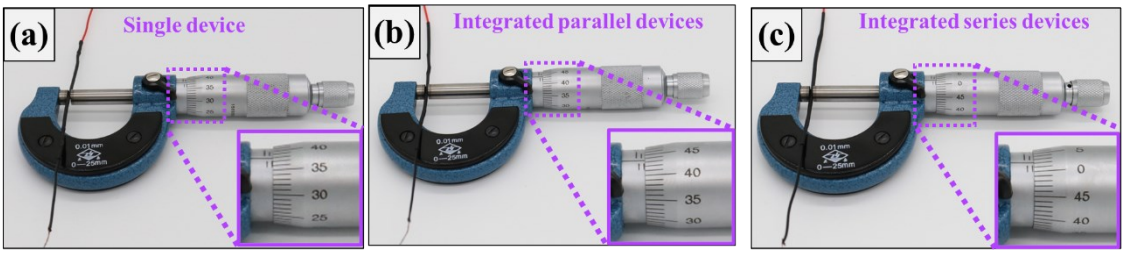

Figure S16. The digital photographs of fiber-shaped single-device, integrated parallel devices and integrated series devices.

Figure S17. Photograph of a red LED illuminated by two single-devices.

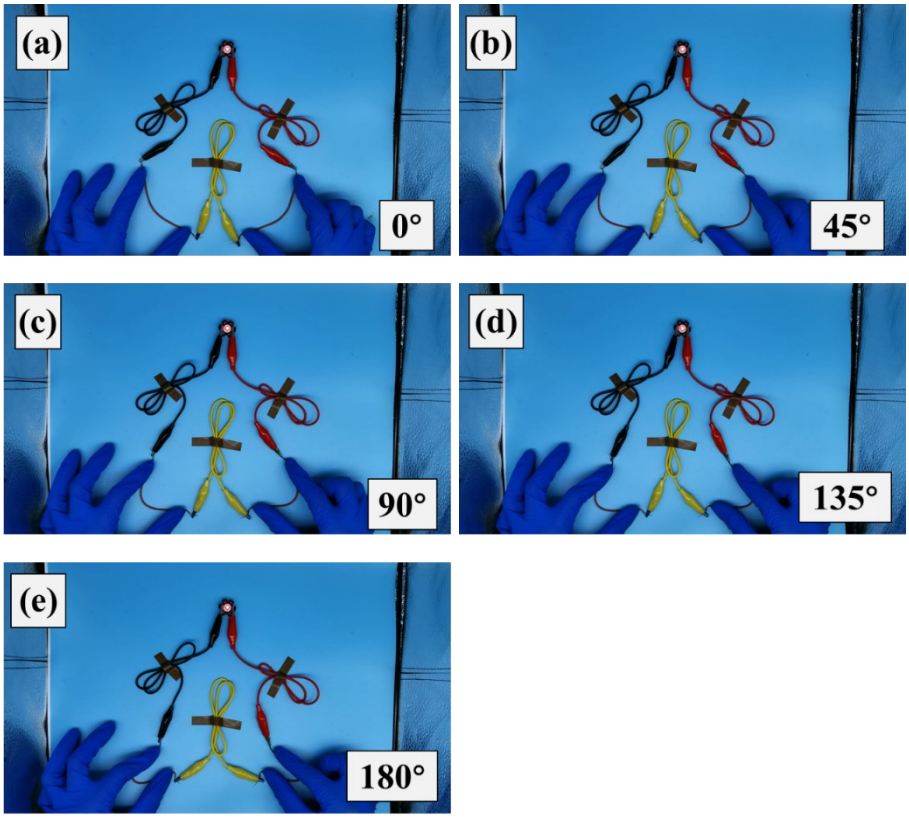

Figure S18. Optical images of lightness of a red LED (powered by two devices in series) changes with different bending angles.

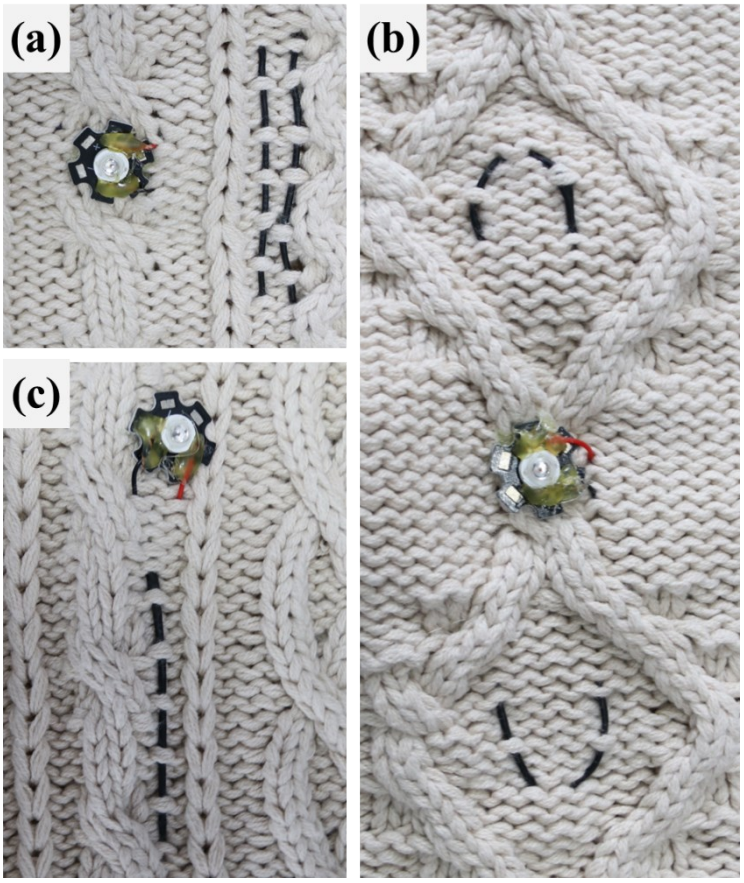

Figure S19. High magnification photographs of practical applications of fiber shaped devices.

Table S1. Comparison of the Specific capacity of our Zn// Mn_2O_3/C zinc-ion battery with other aqueous rechargeable batteries previously reported.

Devices	Specific capacity	Current density	Reference
Zn// α-(Mn_2O_3@MnO_2)	170 mA h g^{-1}	0.5 A g^{-1}	2
Zn// Mn_2O_3	233 mAh g^{-1}	0.3 A g^{-1}	3
Zn// Oc_u-Mn_2O_3	246 mAh g^{-1}	0.05 A g^{-1}	4
Zn// Mn_2O_3/Al_2O_3 composite	289.8 mA h g^{-1}	0.3 A g^{-1}	5
Zn// Mn_2O_3/C	253.1 mAh g^{-1}	0.49 A g^{-1}	This work

Table S2. Comparison of the cycling performances of our assembled ZIBs with other previously work.

Energy storage devices	Cycles	Capacity retention	Refence
MnO_2/C: Zn battery	450	28.34%	6
$ZnNi_{1/2}Mn_{1/2}CoO_4$: Zn battery	200	81.6%	7
MoO_3: Zn	400	70.4	8
MnO_2@A4-type paper: Zn	64	40	9
MnO_2@Ppy @ stainless steel: Deposited Zn@nitin of wire	1000	60	10
MnO_2: Zn	600	79.7	11
MnO_2: Zn	1500	31.8	12
VS_4: Zn	500	85	13
Zn: MnO_2	1000	~60%	14
Zn/VS_2	200	98	15
V_2O_5 nanosheets: Zn	400	67	16
$Zn_3V_2O_7(OH)_2{\cdot}2H2O$ nanowires: Zn	300	68	17
V_6O_{13}/CC:Zn	200	90%	18
Mn_2O_3@C: Zn battery	3000	79.6%	This work

References

1. Y. Huang, J. Mou, W. Liu, X. Wang, L. Dong, F. Kang and C. Xu, *Nano-Micro Lett.*, 2019, **11**, 49.
2. J. Long, F. Yang, J. Cuan, J. Wu, Z. Yang, H. Jiang, R. Song, W. Song, J. Mao and Z. Guo, *ACS Appl. Mater. Inter.*, 2020, **12**, 32526-32535.
3. D. Feng, T.-N. Gao, L. Zhang, B. Guo, S. Song, Z.-A. Qiao and S. Dai, *Nano-Micro Lett.*, 2019, **12**, 14.
4. N. Liu, X. Wu, Y. Yin, A. Chen, C. Zhao, Z. Guo, L. Fan and N. Zhang, *ACS Appl. Mater. Inter.*, 2020, **12**, 28199-28205.
5. L. Gou, K.-L. Mou, X.-Y. Fan, M.-J. Zhao, Y. Wang, D. Xue and D.-L. Li, *Dalton T.*, 2020, **49**, 711-718.
6. G. Li, Z. Huang, J. Chen, F. Yao, J. Liu, O. L. Li, S. Sun and Z. Shi, *J. Mater. Chem. A*, 2020, **8**, 1975-1985.
7. C. Pan, R. Zhang, R. G. Nuzzo and A. A. Gewirth, *Adv. Energy Mater.*, 2018, **8**, 1800589.
8. X. He, H. Zhang, X. Zhao, P. Zhang, M. Chen, Z. Zheng, Z. Han, T. Zhu, Y. Tong and X. Lu, *Adv. Sci.*, 2019, **6**, 1900151.
9. M. H. Alfaruqi, V. Mathew, J. Gim, S. Kim, J. Song, J. P. Baboo, S. H. Choi and J. Kim, *Chem. Mater.*, 2015, **27**, 3609-3620.
10. Z. Wang, Z. Ruan, Z. Liu, Y. Wang, Z. Tang, H. Li, M. Zhu, T. F. Hung, J. Liu, Z. Shi and C. Zhi, *J. Mater. Chem. A*, 2018, **6**, 8549-8557.
11. S. Chen, R. Lan, J. Humphreys and S. Tao, *Energy Storage Materials*, 2020, **28**, 205-215.
12. J. Hao, X. Li, S. Zhang, F. Yang, X. Zeng, S. Zhang, G. Bo, C. Wang and Z. Guo, *Adv. Funct. Mater.*, 2020, **30**, 2001263.
13. Q. Zhu, Q. Xiao, B. Zhang, Z. Yan, X. Liu, S. Chen, Z. Ren and Y. Yu, *J. Mater. Chem. A*, 2020, **8**, 10761-10766.
14. J. Zheng, Q. Zhao, T. Tang, J. Yin, C. D. Quilty, G. D. Renderos, X. Liu, Y. Deng, L. Wang, D. C. Bock, C. Jaye, D. Zhang, E. S. Takeuchi, K. J. Takeuchi, A. C. Marschilok and L. A. Archer, *Science*, 2019, **366**, 645.

15. P. He, M. Yan, G. Zhang, R. Sun, L. Chen, Q. An and L. Mai, *Adv. Energy Mater.*, 2017, **7**, 1601920.
16. J. Zhou, L. Shan, Z. Wu, X. Guo, G. Fang and S. Liang, *Chem. Commun.*, 2018, **54**, 4457-4460.
17. C. Xia, J. Guo, Y. Lei, H. Liang, C. Zhao and H. N. Alshareef, *Adv. Mater.*, 2018, **30**, 1705580.
18. P. He, J. Liu, X. Zhao, Z. Ding, P. Gao and L.-Z. Fan, *J. Mater. Chem. A*, 2020, **8**, 10370-10376.